Electronic Supplementary Information

Large-Gain Low-Voltage and Wideband Organic Photodetectors via Unbalanced Charge Transport

Jianfei Huang,[a,e] Jaewon Lee,[b] Max Schrock,[a] Alana L. Dixon,[a] Alexander T. Lill,[a] Kilwon Cho,[c] Guillermo C. Bazan[d,e,] and Thuc-Quyen Nguyen[a,e,*]*

[a]Center for Polymers and Organic Solids, University of California, Santa Barbara, CA 93106, USA

[b]Department of Chemical Engineering and Applied Chemistry, Chungnam National University, Daejeon, 34134, Republic of Korea

[c]Center for Advanced Soft Electronics, Department of Chemical Engineering, Pohang University of Science and Technology, Pohang, 37673, Republic of Korea

[d]Departments of Chemistry and Chemical Engineering, National University of Singapore, Singapore 117543, Republic of Singapore

[e]Mitsubishi Chemical Center for Advanced Materials, University of California, Santa Barbara, CA 93106, USA

Experimental Section

Materials. PTB7-Th, was purchased from 1-Material. TCNQ was purchased from Sigma-Aldrich. PEDOT:PSS solution was purchased from Ossila (Al 4083). P3HT was obtained from Rieke Metals, Inc. The small-molecule acceptors, COTIC-4F and CO1-4Cl, were synthesized according to the previous work.[1,2] Al-doped ZnO nanoparticle suspension was purchased from Sigma-Aldrich. Indium-tin oxide (ITO) substrates were obtained from Thin Film Devices. Commercial materials were used as received without further purification.

Device fabrication. The ITO substrates were cleaned with deionized water, acetone and isopropanol, respectively. Solutions of PTB7-Th:COTIC-4F:TCNQ (PC-T*x*) with the weight ratio of 1:1.5:*x* (*x* varies from 0 to 0.025) were prepared in chlorobenzene. The fresh solution was kept under stirring at 60 °C for overnight and used the next day to minimize solute aggregation. The cleaned ITO substrates were subject to UV-ozone treatment for 15 min and PEDOT:PSS solution was spun onto the ITO substrates at 2500 rpm for 1 min, followed by thermal annealing at 120 °C for 30 min. Subsequently, the PC-T*x* solution with a concentration of 25 mg/mL was deposited onto the PEDOT:PSS-covered ITO substrates in a nitrogen glovebox by spin coating. The aluminum top electrode was then thermally evaporated onto the active layer under a vacuum level of ~10^{-6} torr. The device area was defined by the overlapping area of the top electrode and pre-patterned ITO bottom electrode, giving a device area of 4.51 mm^2. For the devices with an Al-doped ZnO layer between the active layer and Al top electrode, the Al-doped ZnO nanoparticles suspension was spun onto the PC-T*x* active layer at 3500 rpm prior to deposition of the top electrode. The devices based on PTB7-Th:CO1-4Cl and P3HT:COTIC-4F with 1% TCNQ relative to the weight of the BHJ were prepared similarly. The devices for TLM tests were made with active layers of PC-T0 and PC-T1 under the same processing condition for the photodetectors. The

active layers were deposited on benzocyclobutene-covered SiO_2/Si^{++} substrates, followed by vacuum deposition of 100 nm Al top contacts through shadow masks.

Characterizations. Fourier-transform infrared (FT-IR) spectroscopy of pristine TCNQ and Al vapor treated TCNQ powders were performed using a Perkin Elmer Spectrum Two spectrometer with a universal attenuated total reflectance (UATR) attachment. Contact potential and thin film morphologies were obtained from an Asylum MFP-3D atomic force microscope with amplitude modulation SKPM (AM-SKPM) under an inert atmosphere. A single Au-coated Si tip with a resonant frequency of 300 kHz and a force constant of 40 N m^{-1} was used in a two-pass scanning method. The images were processed using first order image flattening and all images were analyzed on Asylum Research AFM software version 14, programmed using IGOR Pro. The GIWAXS data was collected at the Advanced Light Source at Lawrence Berkeley National Lab on the 7.3.3 beamline. The samples prepared on silicon substrates were scanned with an incidence angle of 0.12° and a photon energy of 10 keV (λ = 1.24 Å), while under a helium environment to minimize beam damage and reduce air scattering. The width of the incident X-ray beam is about 1 mm, and silver behenate was used to calibrate the lengths in the reciprocal space. A 2D detector (PILATUS 2 M from Dectris) with a sample-to-detector distance of 276.9 mm was used to collect the images. The Nika software package for Igor (by Wavemetrics) and the Igor script WAXStools were used to process the image. The current-voltage data were collected with a Keithley 4200 semiconductor characterization system. The EQE was measured with a monochromatic light source with a modulation frequency of 35 Hz. The current signal was amplified with a low-noise pre-amplifier (SRS 570) and recorded with an SR810 DSP lock-in amplifier (Stanford Research System). Calibration was done with reference silicon and germanium photodiodes. For the light intensity-photocurrent measurement, calibrated 940 nm light-emitting diodes (LEDs) were used

as the light source, and the signals from the devices under test were fed to the pre-amplifier and collected with a lock-in amplifier (AMETEK SI 5210). The light intensity was varied by a set of neutral filters. To measure the phototransient behavior of the devices, a function generator (SRS DS345) was employed to supply square-wave AC voltage to the 940 nm LEDs to generate pulsed optical signal. The response from the photodetector was obtained with an oscilloscope (Keysight DSOX3022T).

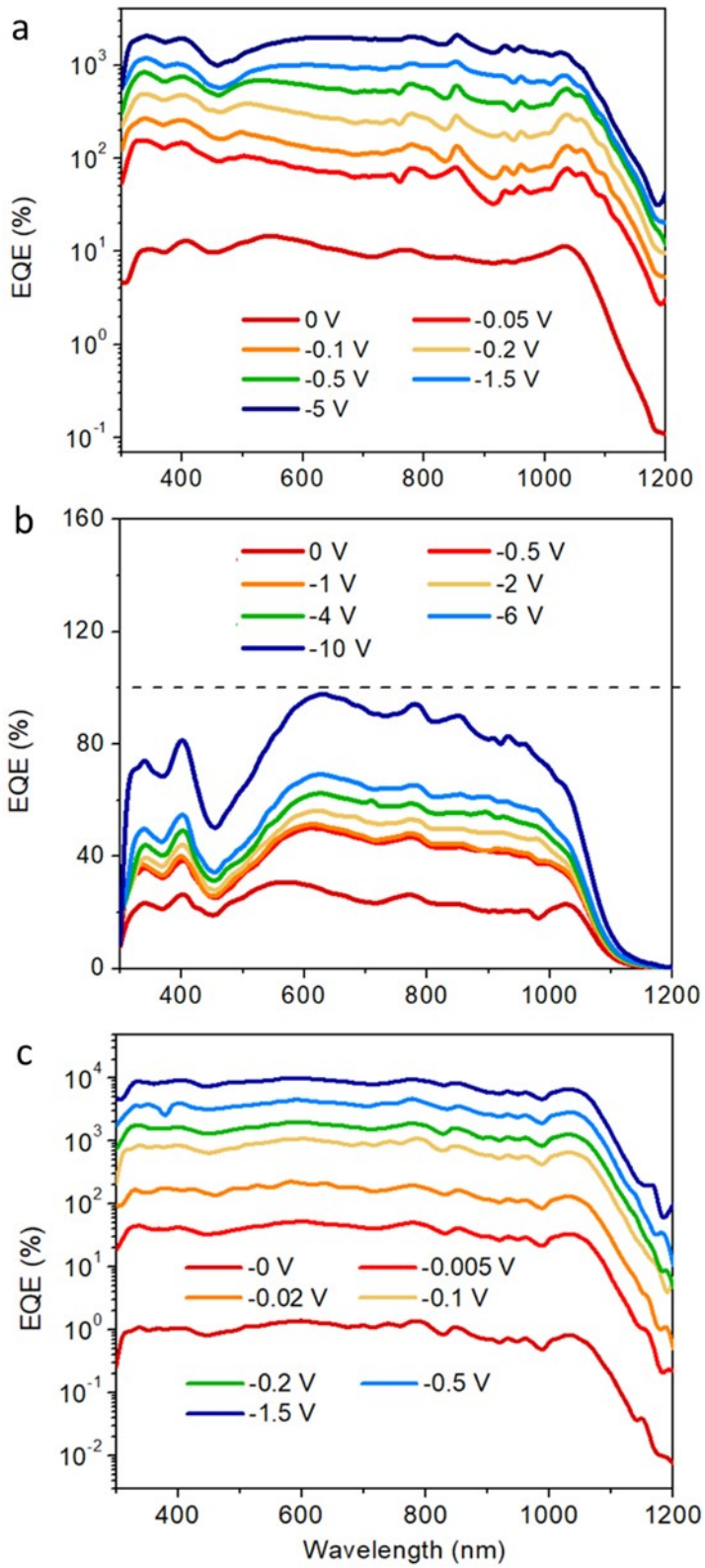

Fig. S1. EQE profiles of (a) PC-T0.3, (b) PC-T0.1 and (c) PC-T1.55 under various biases.

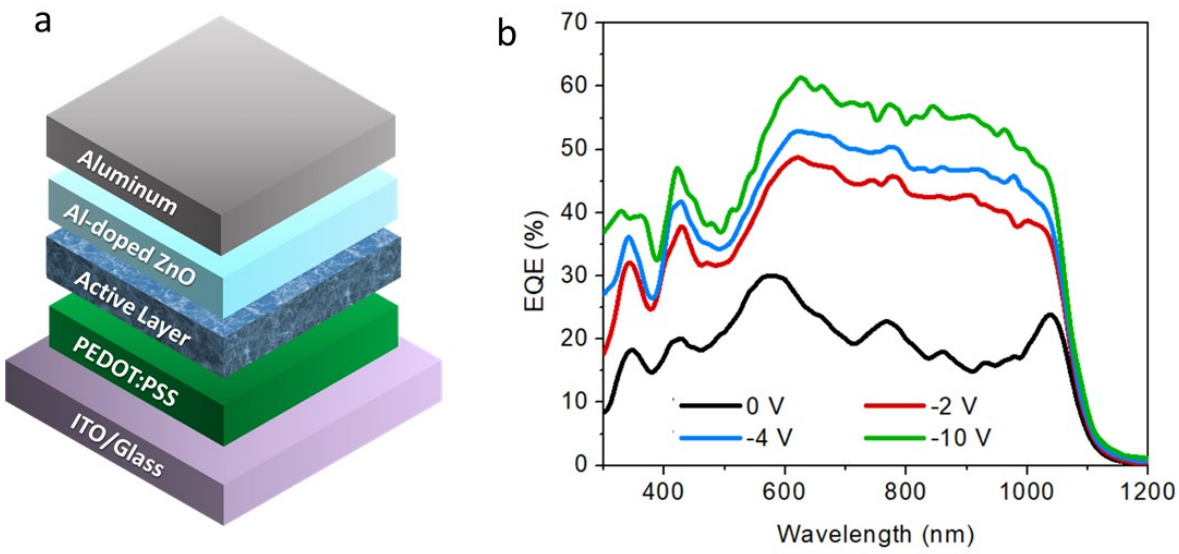

Fig. S2 (a) Device structure and (b) typical EQE spectrum of the device with PC-T1 active layer and solution-processed aluminum-doped zinc oxide nanoparticle layer between the active layer and the top electrode.

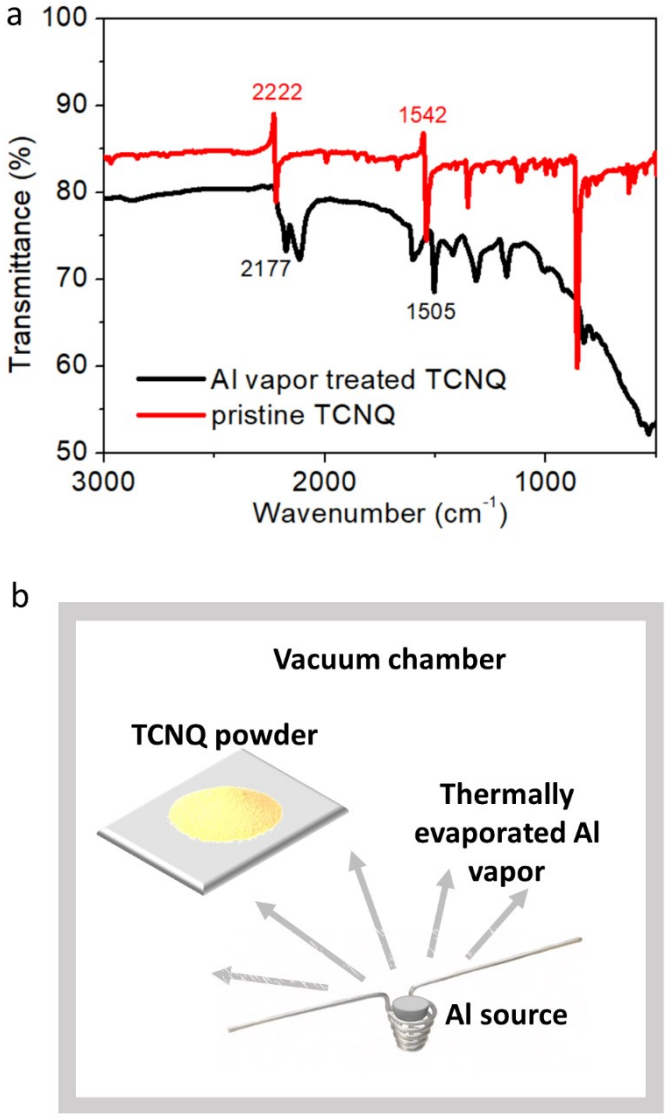

Fig. S3 (a) FTIR spectra of pristine TCNQ and Al vapor treated TCNQ samples. (b) Schematic of preparation of Al vapor treated TCNQ sample. Al vapor treated TCNQ was prepared by placing a boat holding pristine TCNQ powders near an Al source by thermal evaporation.

The C≡N and C=C peaks typical of the reduced form of TCNQ species are identified for the Al vapor treated TCNQ sample at 2177 cm^{-1} and 1505 cm^{-1}, respectively. For pristine the TCNQ sample, the corresponding characteristic signals are found at 2222 cm^{-1} (C≡N) and 1542 cm^{-1} (C=C) for neutral $TCNQ^0$. Such shifts suggest electron transfer from Al to TCNQ and formation of Al-TCNQ complexes during evaporation of the Al electrode atop the TCNQ-containing active layer.[3,4]

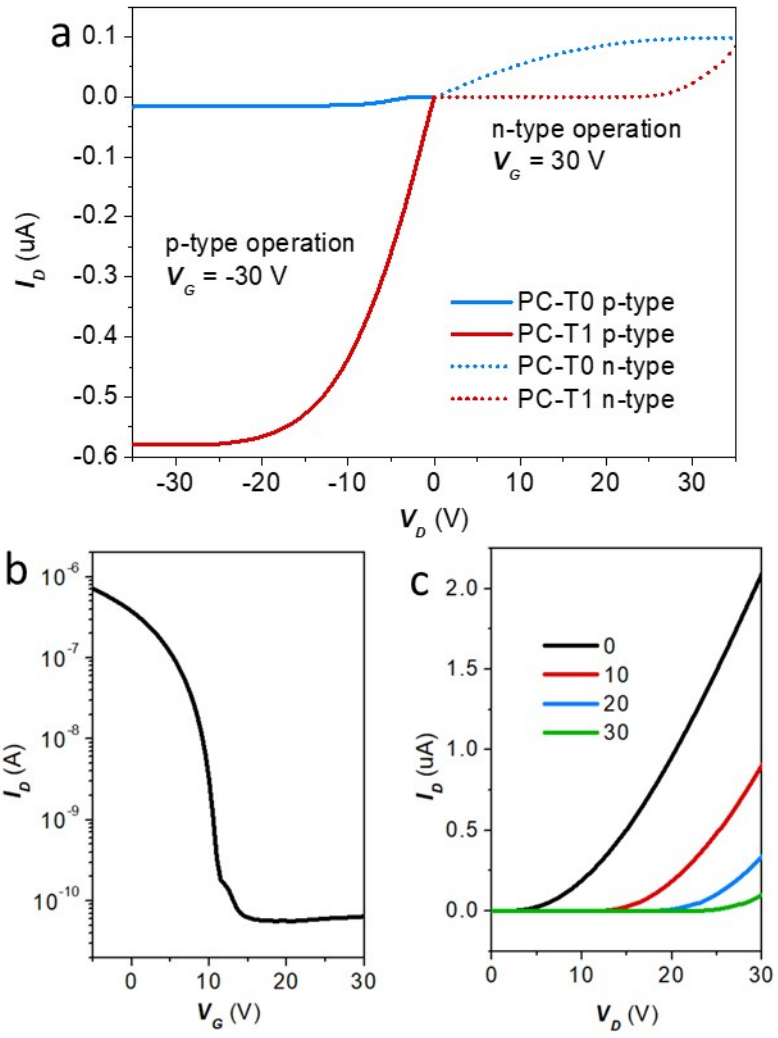

Fig S4. (a) Comparison of n-type and p-type operation output characteristics for FETs based on PC-T0 and PC-T1 films with $|V_G|$ of 30 V. Device channel length is 20 um. (b) Typical transfer and (c) output characteristics for FETs with PC-T1 as the active layer. Channel length is 35 um.

The FETs based on PC-T0 active layer can be operated under both n-type and p-type transport, although the latter is greatly inhibited due to the large mismatch between the Fermi level of Al with the HOMO level of either PTB7-Th or COTIC-4F in the BHJ blend, as manifested by the low drain current in p-type operation of the PC-T0 device. However, when the TCNQ is present, the p-type transport is greatly enhanced as seen by the significantly increased field-effect current, while the n-type transport becomes difficult due to the electron trapping. As shown in Fig. S4a, the n-type transport is inhibited and at larger V_D the hole injection occurs at drain electrode. Consistently, the transfer curve (Fig. S4b) shows that the PC-T1 device cannot be switched on for

n-type transport (in positive V_G), but is easily switched on for p-type transport as the V_G shifts to negative. This is further confirmed by the output characteristics at different V_G (Fig. S4c). With decreased positive V_G values, the degree of the channel being hole-depleted is decreased, and thus a larger drain current from hole transport is found.

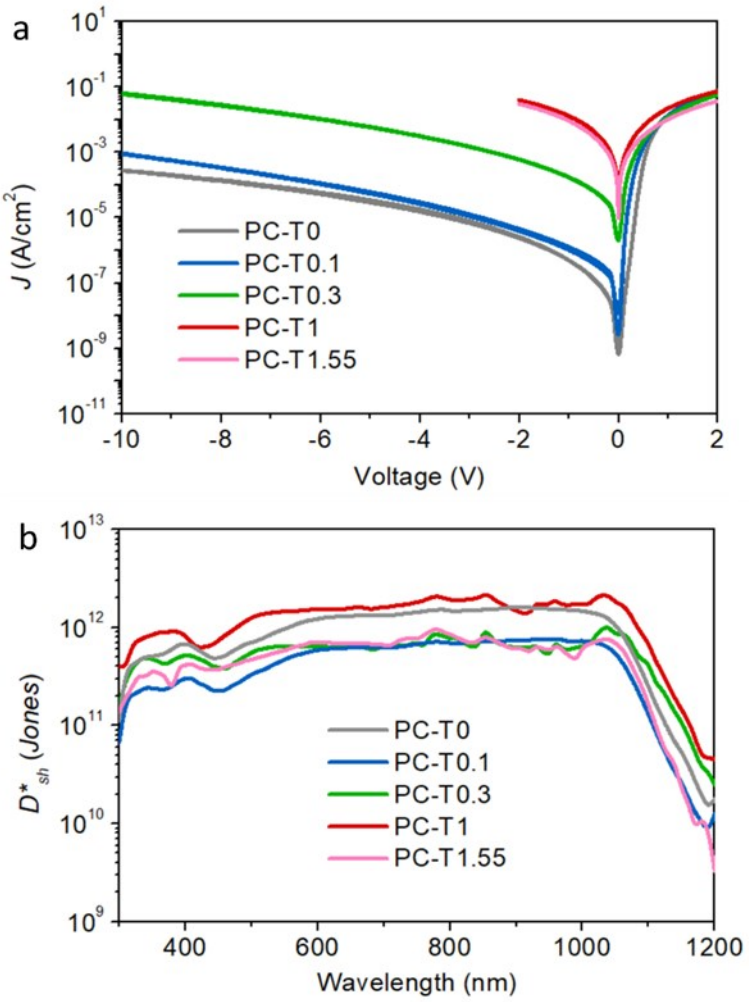

Fig. S5 (a) *J-V* characteristics in the dark of the PC-T*x* devices. (b) Shot noise-limited specific detectivity (D^*_{sh}) at -0.5 V evaluated using the equation $D^*_{sh} = \frac{EQE\ e\lambda}{hc\sqrt{2eJ_d}}$, where e is the elementary charge, λ is the wavelength, h is Planck constant, c is the speed of light, and J_d is the dark current density.

As a result of increase in work function of the Al top electrode and improved hole injection, the dark current increases with the amount of the TCNQ (Fig. S5a). In addition, a gradual loss of typical diode rectification behavior is observed with more TCNQ in presence, indicating a Schottky-to-ohmic conversion of the metal/organic interface. Despite this, the significantly enhanced photoresponse well compensates the increased dark current, rendering comparable peak specific detectivity (D*) over 10^{12} Jones under -0.5 V for PC-T1 (Fig. S5b). Hence, the gain photodetectors still offer comparable *D** to the non-gain counterpart, yet offering much higher photoresponsivity.

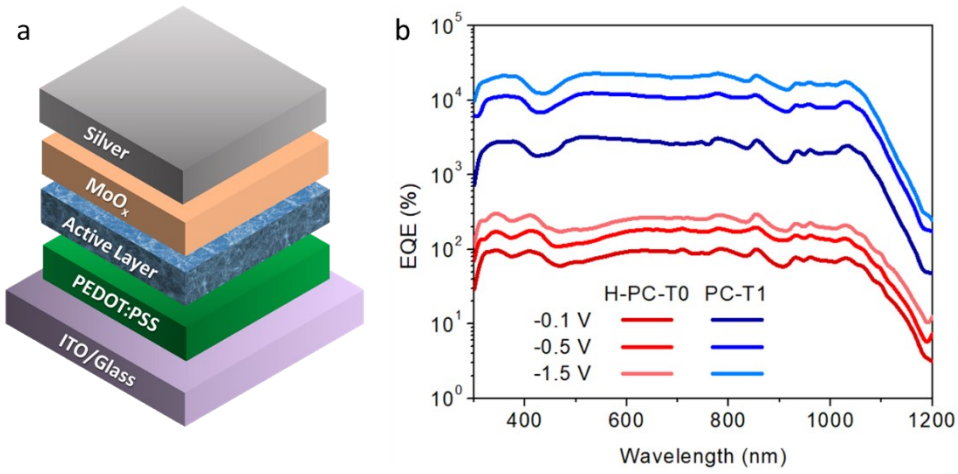

Fig. S6 (a) Device structure and (b) spectral EQE of H-PC-T0 device with MoO_x/Ag as the top electrode compared with PC-T1 device.

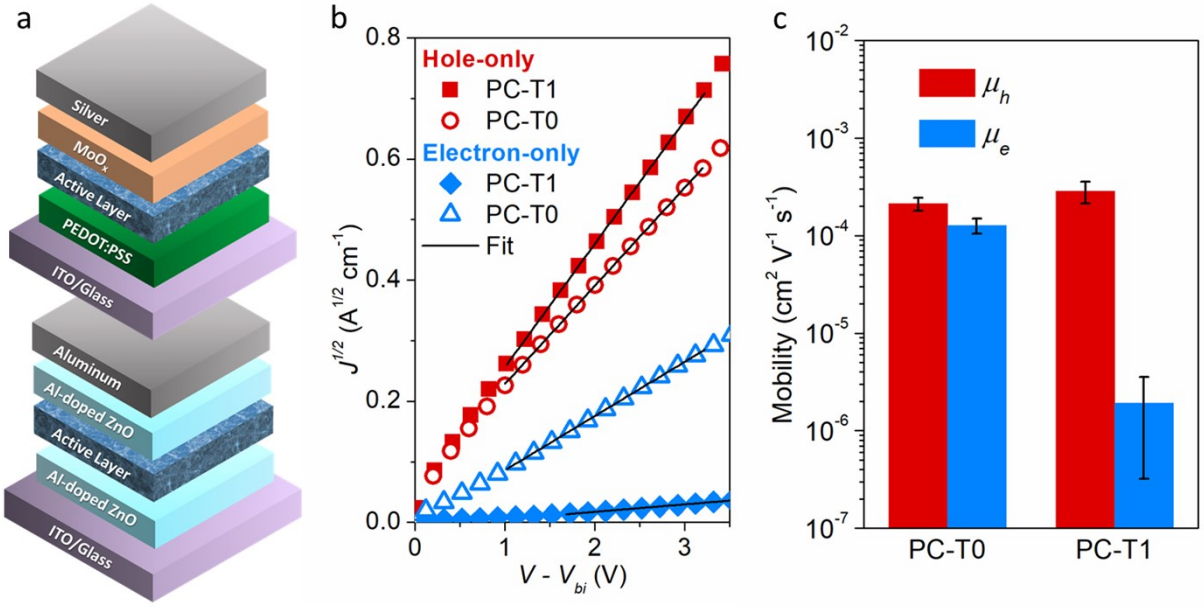

Fig. S7 (a) Device structure of the hole-only (upper) and electron-only (lower) diodes. Specifically, for electron-only diode, the active layer is sandwiched between Al-doped ZnO layers to prevent the interaction between the interfacial TCNQ and Al electrode. (b) Plot of $J^{1/2}$ vs (V_a - V_{bi}) of the single-carrier diodes. (c) Hole mobility (μ_h) and electron mobility (μ_e) for the PC-T0 and PC-T1 devices. The mobilities were according to Mott-Gurney law ($J = \frac{9\varepsilon\mu(V_a + V_{bi})^2}{8L^3}$), where J, ε, μ, V_a, V_{bi} and L are the current density, permittivity, mobility, applied voltage, built-in voltage and thickness of the film, respectively.

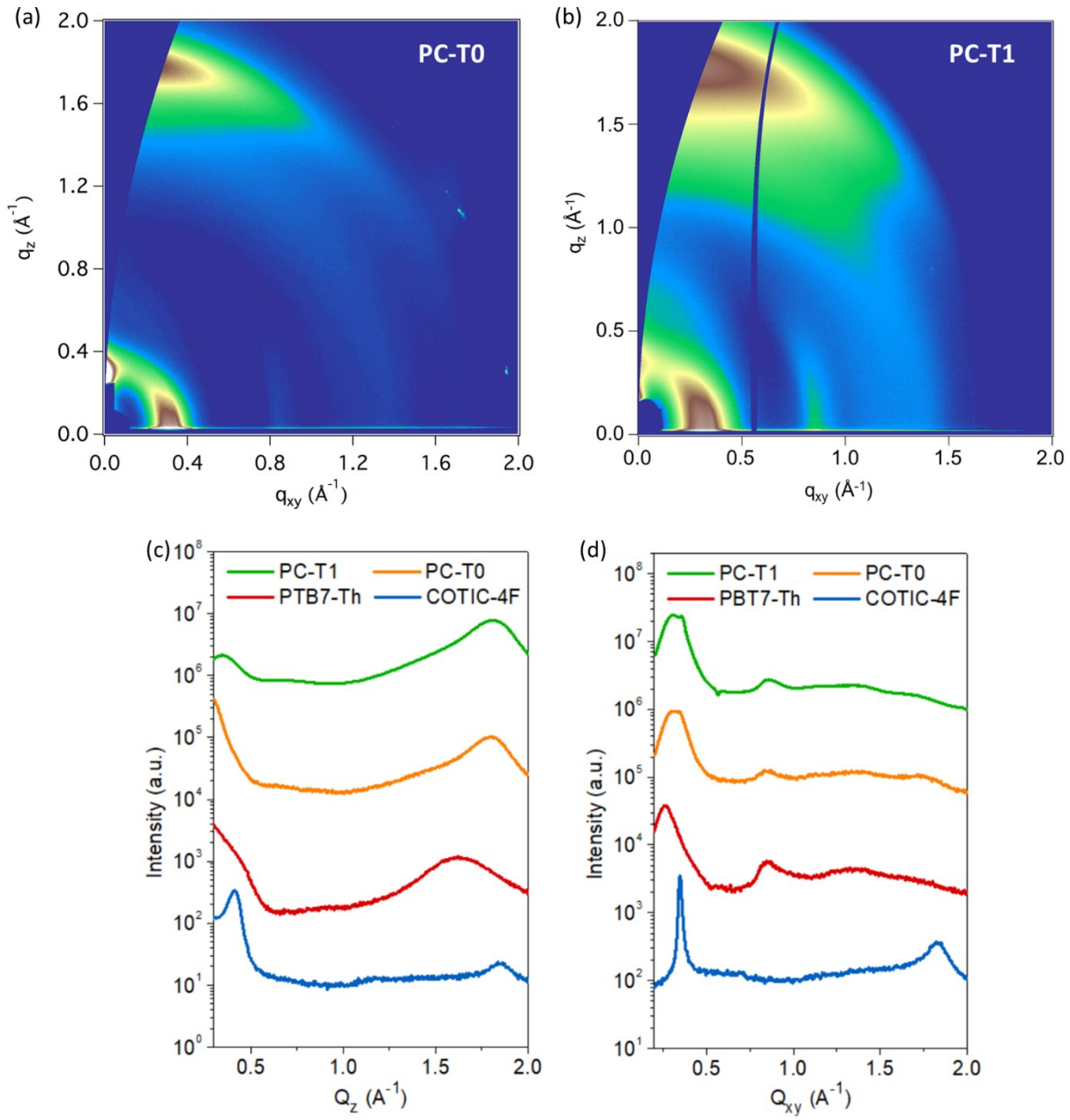

Fig. S8 2D GIWAXS images of (a) PC-T0 and (b) PC-T1 films. (c) Out-of-plane and (d) in-plane line-cut features of PC-T0 (orange), PC-T1 (green), PTB7-Th (red) and COTIC-4F (blue) films. Data of PC-T0 and the neat films are extracted from our previous work.[5]

The overall GIWAXS features of PC-T1 film are very similar to those of the PC-T0 film. Notably, no distinct new features arise in either lamellar or π-π stacking directions for PC-T1 when compared to PC-T0. This implies the small quantity of TCNQ does not form a separate crystalline phase in the blend large enough to be distinguishable by GIWAXS, which is consistent with the similar morphologies of the two films as characterized by AFM (Fig. S10). It is noted that both

films show a preferential face-on orientation and have very close out-of-plane π-π stacking distances, further marking their similar molecular packing behavior for the vertical charge transport (Table S1). Addition of TCNQ only slightly disrupts the ordering within the blend film, as indicated by the decreased coherence lengths (L_c). Since the main charge transport is normal to the substrate for vertical devices, we should mainly consider the high q_z features. It is fond that L_c which corresponds to the lower-LUMO main component COTIC-4F's (q_z 1.85 Å^{-1}) cannot be confirmed to decrease with addition of TCNQ. In addition, for the vertical hole transport, one finds the q_z feature around 1.79 Å^{-1} has a higher L_c for PC-T0, while in fact the hole mobility is slightly higher for PC-T1. Thus, the observed morphology change cannot be viewed as posing a major impact on drastically decreased electron mobility.

Table S1. Summary of the GIWAXS scattering patterns[(a)]

q_{xy} (Å^{-1})	d (nm)	L_c (nm)	q_z (Å^{-1})	d (nm)	L_c (nm)
PC-T1					
0.31	2.02	2.49	0.34	1.83	2.42
0.36	1.76	5.26	1.79	0.35	2.29
			1.85	0.34	4.20
PC-T0					
0.28	2.26	7.18	0.314	2.00	-
0.34	1.84	6.22	1.794	0.35	2.92
PTB7-Th					
0.27	2.37	5.42	1.63	0.39	1.63
COTIC-4F					
0.35	1.8	29.3	0.42	1.51	5.15
1.83	0.34	6.23	1.85	0.34	5.35

[(a)]L_c were calculated using the Scherrer equation are the distance over which the molecular order producing each scattering feature is maintained within the film. Data for PC-T0, PTB7-Th and COTIC-4F are extracted from our previous work.[5]

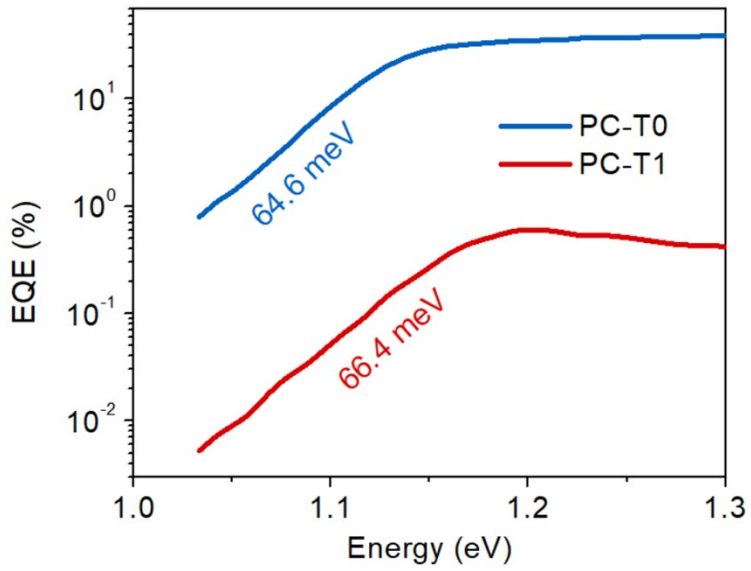

Fig. S9 EQE spectra of PC-T0 and PC-T1 devices near the sub bandgap region and their Urbach energies.

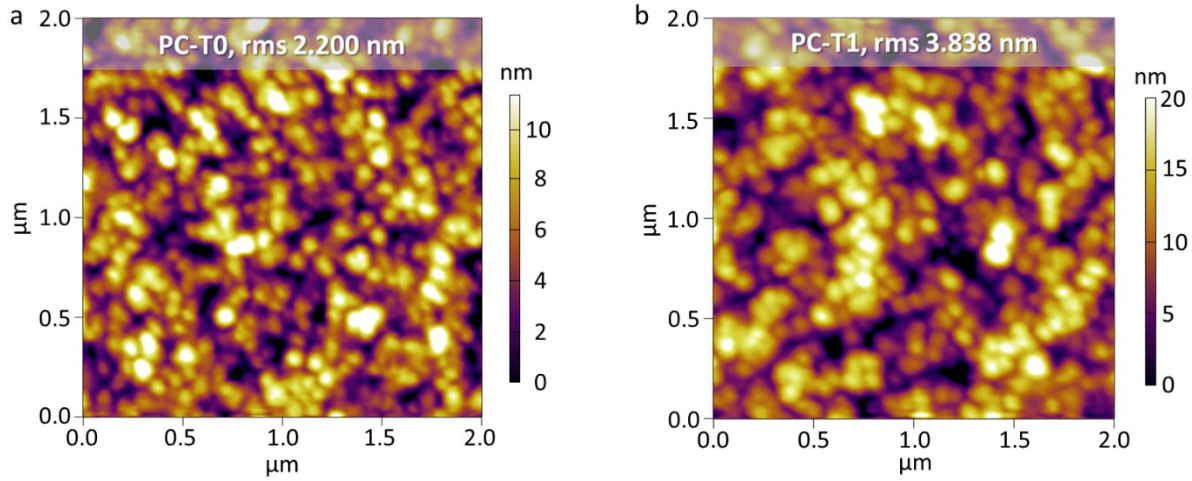

Fig. S10 AFM height images of the active layers of (a) PC-T0 and (b) PC-T1.

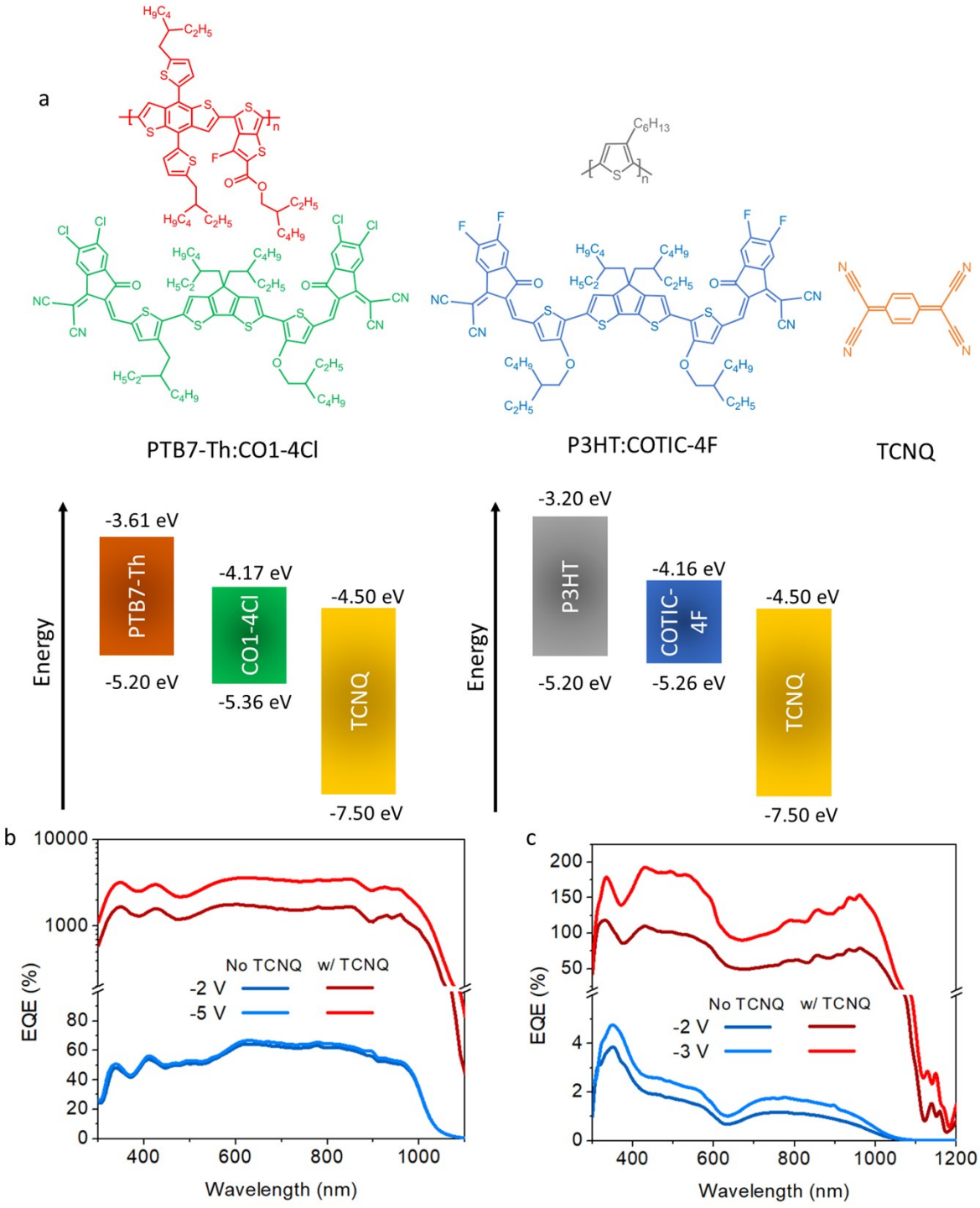

Fig. S11 (a) Chemical structures and energy diagrams of the materials in the other two blends. EQE profiles of devices with active layers of (b) PTB7-Th:CO1-4Cl:TCNQ (1:1.5:0.025 and 1:1.5:0 weight ratio) and (c) P3HT:COTIC-4F:TCNQ (1:1:0.02 and 1:1:0 weight ratio). The device preparation is similar to that of PC-T*x* devices except that the corresponding the donor or acceptor was varied.

References

1 J. Lee, S.-J. Ko, H. Lee, J. Huang, Z. Zhu, M. Seifrid, J. Vollbrecht, V. V. Brus, A. Karki, H. Wang, K. Cho, T.-Q. Nguyen and G. C. Bazan, *ACS Energy Lett*. 2019, **4**, 1401.

2 J. Huang, J. Lee, J. Vollbrecht, V. V. Brus, A. L. Dixon, D. X. Cao, Z. Zhu, Z. Du, H. Wang, K. Cho, G. C. Bazan and T.-Q. Nguyen, *Adv. Mater.* 2020, **32**, 1906027.

3 A. Pearson, A. P. O'Mullane, S. K. Bhargava and V. Bansal, *Inorg*. *Chem*. 2012, **51**, 8791.

4 R. Ramanathan, A. E. Kandjani, S. Walia, S. Balendhran, S. K. Bhargava, K. Kalantar-zadeh and V. Bansal, *RSC Adv.* 2013, **3**, 17654.

5 J. Lee, S.-J. Ko, M. Seifrid, H. Lee, B. R. Luginbuhl, A. Karki, M. Ford, K. Rosenthal, K. Cho, T.-Q. Nguyen and G. C. Bazan, *Adv. Energy Mater.* 2018, **8**, 1801212.